Contrasting Kinetics of Highly Similar Chloroalkane Reductive Dehalogenases

Katherine J. Picott[a] *and Elizabeth A. Edwards*[a*]

[a]Department of Chemical Engineering and Applied Chemistry, University of Toronto, Toronto, Ontario, Canada M5S 3E5

*Corresponding Author: Elizabeth A. Edwards, e-mail: elizabeth.edwards@utoronto.ca; Tel. (+1) 416 946 3506; Fax (+1) 416 978 8605.

ABSTRACT

Chloroform and trichloroethanes are pervasive groundwater contaminants for which bioremediation has been an effective treatment strategy. Reductive dehalogenase (RDase) enzymes from organohalide-respiring bacteria are essential for their remediation under anaerobic conditions. RDases are responsible for dehalogenating these chlorinated solvents, leading to their removal. This work explores the kinetic characteristics of three closely related *Dehalobacter* chloroalkane-reductases—TmrA, CfrA, and AcdA—and identifies differences between their activity on chloroform (CF), 1,1,1-trichloroethane (TCA), and 1,1,2-TCA. The side-by-side comparison of these enzymes has emphasized that TmrA and AcdA are specialized toward CF with both having 4-fold higher maximum specific activity (V_{max}) on CF than 1,1,1-TCA, whereas, CfrA has very similar rates on both CF and 1,1,1-TCA. AcdA is the most sensitive to substrate inhibition by CF and 1,1,2-TCA, and inhibition by a common co-contaminant trichloroethene. Finally, the reduction of 1,1,2-TCA, which can produce both 1,2-dichloroethane and vinyl chloride, was assessed for each enzyme. Interestingly, each enzyme has a distinct preference for the major product it produces, indicating a favoured reaction pathway. Despite over 95% sequence identity, TmrA, CfrA, and AcdA exhibit substantial differences in kinetic behaviour, highlighting the importance of understanding such nuances for informed bioremediation strategies.

KEYWORDS

Dehalobacter, chloroform, trichloroethane, enzyme kinetics, reaction rate, bioremediation, dechlorination

SYNOPSIS

Three similar dechlorinating enzymes were found to have distinct reaction rates and levels of sensitivity to inhibition. These differences have implications for the enzymes' use in bioremediation.

37 **INTRODUCTION**

38 Chloroform (CF) and isomers of trichloroethane (TCA) are widespread groundwater
39 contaminants that are included on the Agency for Toxic Substance and Disease Registry's
40 (ATSDR) Substance Priority List [1,2]. Bioaugmentation is a convenient and economical method of
41 remediating sites contaminated with these compounds [2–5]. There are several bioaugmentation
42 cultures that target CF, 1,1,1-TCA, and 1,1,2-TCA [6–11].

43 These bioaugmentation cultures are all mixed communities that contain organohalide-
44 respirers *Dehalobacter* and *Desulfitobacterium* [7,8,11–14], which use reductive dehalogenases
45 (RDases) as the terminal enzyme in their electron transport chain [15]. RDases catalyze the reduction
46 of specific organohalide compounds—specificity depends on the enzyme itself—and in doing so,
47 they remove one halogen through a hydrogenolysis pathway or two halogens through a
48 dihaloelimination pathway [15]. All RDases require a cobamide and two iron-sulfur clusters as
49 cofactors [15]. RDases with high protein sequence identity (>90%) are classified into ortholog groups
50 (OGs), members of each OG generally target substrates that are structurally similar; e.g.
51 chloroalkanes [16,17]. However, it has been observed that similar RDases can be tuned to have
52 uniquely specialized activity [18–20], yet the factors contributing to these differences are largely
53 unexplored.

54 OG 97 comprises one *Desulfitobacterium* and six *Dehalobacter* RDases that dechlorinate
55 halomethanes and chloroethanes [7,9,10,20–22]. OG 97 members are particularly intriguing because
56 they are the only identified RDases capable of dechlorinating CF and 1,1,1-TCA, and they display
57 variation in substrate preferences despite many sharing over 95% amino acid sequence identity
58 [7,9,10,20–22]. The substrate preferences of the enzymes correlate well with the respiration of their
59 native organism [7,9,10,20–22], indicating that the RDase activity influences respiratory function.

60 Notably, *Dehalobacter* strains producing different RDases—TmrA, CfrA, AcdA, and RdhA
61 D8M_v2_40029—exhibit varying CF isotope fractionation patterns, potentially indicating
62 differences in the enzymatic mechanisms [10,23,24].

63 This study focuses on TmrA from *Dehalobacter* sp. UNSWDHB in CFH2 [21,25], CfrA from
64 *Dehalobacter* sp. CF in ACT-3 [20], and AcdA from a *Dehalobacter* sp. in the enrichment SC05-
65 UT—each found in deployed bioaugmentation cultures [14,22]. RdhA D8M_v2_40029, which shows
66 similarly suppressed carbon isotope fractionation patterns to TmrA and AcdA [10,23,24], was not
67 included. Previous reports on TmrA, CfrA, and AcdA show similar activity on CF, 1,1,1-TCA,
68 and 1,1,2-TCA; TmrA and AcdA also act on 1,1-dichloroethane (DCA), whereas CfrA does not
69 [20–22,26,27]. The kinetics of TmrA and CfrA have been evaluated using cell-free extracts and purified
70 TmrA on select substrates [6,21,28,29]. However, these studies were conducted under different
71 conditions [6,21,28,29], limiting the ability to correlate kinetic data with the observed activity
72 discrepancies. A side-by-side kinetic comparison with these purified chloroalkane reductases has
73 not yet been conducted but could provide valuable insights into the catalytic differences among
74 these closely related enzymes. Gaining a deeper understanding of RDase biochemistry benefits
75 bioremediation practitioners by improving predictions of substrate degradation rates, byproduct
76 formation, and potential inhibition.

77 The recent ability to heterologously express these enzymes in a common host enables a
78 direct comparison [26]. Here, we analyze the kinetics of heterologously produced TmrA, CfrA, and
79 AcdA against three substrates: CF, 1,1,1-TCA, and 1,1,2-TCA. We also compare their sensitivity
80 to inhibition by a common co-contaminant, trichloroethene (TCE), and examine structural features
81 that could contribute to the observed differences.

82

83 **MATERIALS AND METHODS**

84 ***Materials***

85 All chemicals, unless otherwise stated, BugBuster®, and filter tubes were purchased from
86 MilliporeSigma (Burlington, MA, USA). All growth media, antibiotics, and induction agents were
87 purchased from BioShop Canada Inc. (Burlington, ON, Canada). Bradford reagent was purchased
88 from Bio-Rad Laboratories Ltd. (Hercules, CA, USA). All glass syringes were from Hamilton
89 Company (Reno, NV, USA). Steel washers were purchased from Amazon.ca (ASIN:
90 B081L91F6N). All gasses were supplied from Linde Canada Inc. (Mississauga, ON, Canada). A
91 Coy vinyl anaerobic chamber was maintained with an anaerobic atmosphere of 10% CO_2/2-3%
92 H_2/Bal. N_2 (v/v) (Coy Laboratory Products Inc., Grass Lake, MI, USA); this is referred to as a
93 glovebox throughout. Gas chromatography materials were purchased from Agilent Technologies
94 (Santa Clara, CA, USA).

95 ***Enzyme Expression***

96 Three RDases were heterologously expressed in *Escherichia coli*: TmrA (accession:
97 WP_034377773) from *Dehalobacter* sp. UNSWDHB [21], CfrA (AFV05253) from *Dehalobacter*
98 sp. CF [20], and AcdA from a *Dehalobacter* in the SC05-UT enrichment culture (XCH81453) [22].
99 The construction of the expression plasmids *p15TVL-tmrA*, *p15TVL-cfrA*, and *p15TVL-acdA,*
100 enzyme expression, and partial purification have been described elsewhere [22,26]. Minor
101 modifications to the protocol are: lysogeny broth (LB) media was used, and Triton X-100 and
102 glycerol were removed from the wash, elution, and storage buffers. [22,26]. Each expression plasmid
103 was expressed with *pBAD42-BtuCEDFB* in *E. coli* BL21(DE3) *cat-araC*-P_{BAD}-*suf*, *ΔiscR::kan,*
104 *ΔhimA::*Tet^R [30,31]. The *pBAD42-BtuCEDFB* plasmid was gifted by the Booker Lab (Pennsylvania
105 State University, PA, USA). The *E. coli* strain was gifted by the Antony and Kiley Labs (St. Louis

106 University School of Medicine, MO, USA; University of Wisconsin-Madison, WI, USA). All
107 plasmids are in Table S1 and a detailed methodology can be found in Supplemental Text S1.

108 The protein concentration was measured by Bradford assay [32], and the purity was estimated
109 by sodium dodecylsulfate polyacrylamide gel electrophoresis (SDS-PAGE) using Image Lab 6.1
110 software (2022, Bio-Rad Laboratories, Inc.), (Figure S1). The standard deviation of triplicate
111 protein concentration measurements was incorporated into the enzyme activity error (Table S2).

112 ***Kinetic Experimental Method Design and Assumptions***

113 The substrates and products in these reactions are volatile. During preliminary assay
114 development (data not shown), we found that using bottles with headspace produced less
115 consistent mass balances than glass gas-tight syringes without headspace. This is likely due to the
116 short incubation time and frequent sampling invalidating the gas-liquid equilibrium assumption.
117 The final iteration of the assay was conducted in the barrel of a 1-mL glass gas-tight Hamilton
118 syringe. The total assay volume was sampled and analyzed by gas chromatography-flame
119 ionization detection (GC-FID). Given the consistent mass balance we assume that no substrate or
120 product is lost, and the initial amount of substrate was calculated from the amount of product and
121 remaining substrate.

122 The elimination of the headspace, in turn, reduced mixing in the reaction, as observed with
123 highly variable reaction rates in initial trials. We added a small stainless-steel washer inside the
124 syringe barrel as a physical mixer (inspired by Criddle, 1989 [33]) which improved consistency. We
125 assume that these reactions are well-mixed and that the rates are governed by the enzymatic rate-
126 limiting step.

127 Kinetic assays were conducted assuming the chlorinated solvent was the only limiting
128 substrate. RDases depend on an external supply of electrons for catalysis. If the electron donor

129 were limiting (i.e., not in excess of the target substrate), then the apparent rate would be
130 underestimated.

131 Detailed descriptions of the assay setup, data analysis, and kinetic model assessment are
132 provided in Supplemental Texts S2-4. It is important to note that in the native *Dehalobacter*, the
133 rate-limiting step of respiration may be the supply of electrons through the electron transport chain
134 rather than the RDase activity, as suggested previously [29,34]. Our study focuses solely on the rate
135 dictated by the dehalogenation of the supplied organohalide substrate. Additionally, the reactions
136 were performed at room temperature, but the exact temperature could not be controlled in the
137 glovebox and varied between 20–25°C (discussed further in Supplemental Text S5). We will only
138 compare assays performed at the same recorded temperature.

139 ***Kinetic Assay – Vial Set-up***

140 All kinetic assays were performed in an anaerobic glovebox. All materials were
141 equilibrated in the glovebox atmosphere for at least 48 hr before use. A series of vials were used
142 to prepare the reaction buffer for 15 different substrate concentrations with one substrate-free vial
143 to produce a full Michaelis-Menten curve. The reactions themselves took place in glass syringes—
144 the prepared buffer was taken from the vial and the desired enzyme was added to the syringe
145 afterward to keep the stock buffer clean. Four reactions total were done using the same stock buffer
146 vial (enzyme-free negative control, TmrA, CfrA, and AcdA).

147 The assay buffer and substrate mixtures were prepared in sixteen 11-mL vials with mininert
148 caps. Each vial was prepared so that the final liquid volume would be 6 mL with 5 mL headspace.
149 Reaction buffer containing 50 mM Tris-HCl (pH 7.5) and 1 mM methyl viologen (MV) was added
150 to each of the vials, the vials were capped, and the substrate was delivered to the desired
151 concentration from either a saturated water stock or the neat substrate using a gas-tight glass

152 syringe (Table S3). Target aqueous substrate concentration ranges were 10 μM–1.5 mM
153 chloroform (CF), 5 μM–2 mM 1,1,1-trichloroethane (TCA), and 10 μM–5 mM 1,1,2-TCA.
154 However, the actual initial substrate concentration was calculated by summing the remaining
155 substrate and the product measured by GC-FID. All vials were equilibrated overnight. After
156 equilibration, the reductant Ti(III) citrate (pH 7) was added to each vial to a final concentration of
157 5 mM. This was added directly before the assays to prevent premature oxidation of the reductant.
158 Further details of the reaction vial setup and the assay procedure can be found in Supplemental
159 Text S2.

160 Trichloroethene (TCE) was tested as an inhibitor for CF dechlorination. Glass bottles (255
161 mL) with mininert caps were set up with 60 mL of the buffer (50 mM Tris-HCl [pH 7.5] and 1
162 mM MV). TCE was delivered to a concentration of 50 μM using a TCE-saturated water stock. The
163 stock solution was equilibrated overnight and then aliquoted to the 11-mL reaction mixture vials
164 to all have the same amount of TCE. The substrate, CF, and Ti(III) citrate were delivered into the
165 vials as previously stated.

166 ***Kinetic Assay – Reaction***

167 Purified RDases were thawed on ice and diluted in 50 mM Tris-HCl (pH 7.5) to an RDase
168 concentration of 100 nM. Four—one for each enzyme and an enzyme-free control—1-mL glass,
169 gas-tight Hamilton syringes with a flat M1.6 (4 mm diameter, 0.3 mm thick) stainless steel washer
170 inside the barrel of the syringe were used to perform the reactions. The reactions were performed
171 by taking up 900 μL of the assay buffer from the prepared reaction mixture vial and then 100 μL
172 of the diluted enzyme, or buffer for the enzyme-free controls. The syringe was inverted
173 continuously during the incubation, allowing the washer to move through the barrel and physically
174 mix the solution. The reactions were run for 2 min for CF and 1,1,1-TCA assays, and 5 min for

175 the 1,1,2-TCA assays. At the end of the incubation, the 1-mL reaction was injected via a submerged
176 needle into 5 mL HCl acidified water (pH <2) in an 11-mL GC headspace autosampler vial and
177 immediately sealed by crimping with a Teflon-coated septum. The assays were always carried out
178 in order of the lowest substrate concentration to the highest concentration. The same syringe was
179 used for each enzyme or control and washed between reactions with 1 mL of anaerobic acidified
180 water and 1 mL of anaerobic double-deionized water. A schematic of the reaction procedure is in
181 Figure S2.

182 The 1,1,1-TCA kinetic curve was constructed using two sets of data and outliers were
183 identified and removed. Outliers occurred when 1,1,1-TCA was delivered using larger volumes
184 (>250 μL) of saturated stock which caused depletion of the electron donor. The outliers were
185 identified visually by the oxidation of methyl viologen in the buffer vial and if 1,1-dichloroethene
186 (DCE) was present in the negative controls. 1,1,1-TCA is unstable in water and can undergo β-
187 elimination to form 1,1-DCE and hydrolysis to form acetic acid [35,36], which does not interfere with
188 the assay, but 1,1-DCE presence correlated with the observed abiotic oxidation. In these cases, the
189 catalysis is limited by electron supply and the enzyme rate is underestimated. Increasing the
190 number of reactions performed for 1,1,1-TCA and using fresh substrate stocks gave more
191 confidence in the model fit despite the uneven coverage along the Michaelis-Menten curve.

192 All raw data (including outliers) for each kinetic trial is available in Table S4. Negative
193 control data and raw product masses for each reaction are in Supplemental Text S6.

194 ***Analytical procedures (gas chromatography)***

195 Analysis of substrates and products was carried out by GC-FID following the same
196 methods as previously described [22,26], full details are in Supplemental Text S2.

197

198 ***Data processing***

199 The sum of the remaining substrate and products was used to determine the initial substrate
200 concentration in each reaction. The rate was determined by dividing the amount of product (nmol
201 or mg) by the assay time (s) and the mass of RDase in the assay (mg). Error in the protein
202 concentration and an estimated 2-3 s variance for the incubation time were used as uncertainty in
203 the rate values (Table S4).

204 ***Kinetic model fitting***

205 The kinetic data were plotted in Python3 and fit with various Michaelis-Menten kinetic
206 models with and without inhibition using the LMFIT package [37]. The equations of the models
207 tested and their assessment are described in Supplemental Texts S3 and S4. Models were produced
208 using the least squares method and included experimental error in the residual calculation. Data
209 for CF, 1,1,1-TCA, and 1,1,2-TCA without external inhibitors were fit to a typical Michaelis-
210 Menten kinetic expression with and without a term for substrate inhibition. The presence of
211 substrate inhibition was determined by the model of best fit. The best-fit model was selected based
212 on reducing the R^2, Akaike Information Criterion, and the standard deviation of the residuals. The
213 kinetic parameters V_{max} (nmol/s/mg), K_M (μM), and $K_{I,sub}$ (μM; if applicable) were extracted from
214 the models. The k_{cat} (s^{-1}) was calculated by multiplying the V_{max} by the mass of the protein (48 kDa;
215 48 000 g/mol) to convert the protein mass from mg to nmol. All calculated kinetic parameters—
216 in μM and mg/L units—and fit evaluations can be found in Tables S5-S7.

217 To determine the inhibition constant, $K_{I,inh}$, of TCE, first, the V_{max}, K_M, and $K_{I,sub}$ (if
218 applicable) values were determined by the uninhibited CF assay performed on the same day. These
219 values were then set as constants and the TCE-inhibited kinetic data was fit with models for
220 competitive, non-competitive, and uncompetitive inhibition. The best-fit model—selected using

221 the same criteria above—was used to estimate the $K_{I,inh}$. All model assessments can be found in
222 Table S8.

223 Kinetic analysis of 1,1,2-TCA was performed differently than the other substrates because
224 two products are formed (scheme in Figure S3B). The K_M and $K_{I,sub}$ were calculated by modelling
225 the overall 1,1,2-TCA consumption. The reaction rates for each product were then determined by
226 setting K_M and $K_{I,sub}$ as the values determined from the overall rate. A detailed discussion about
227 the 1,1,2-TCA kinetic analysis can be found in Supplemental Text S3.

228 ***Protein Models***

229 Protein models of TmrA and CfrA were retrieved from AlphaFill [38]. AlphaFill contains a
230 database of AlphaFold2 models of all sequences available in UniProt and docks cofactors into the
231 models based on homology to known crystal structures [38,39]. Structures for TmrA and CfrA with
232 cobalamin and two iron-sulfur clusters were extracted and further relaxed using YASARA energy
233 minimization server [40]. The AcdA model was generated directly from AlphaFold2 without the
234 cofactors. The crystal structure of PceA (PBD ID: 4ur0) was used as a comparison of the conserved
235 active site residues [41]. All structures were visualized and analyzed using PyMOL Molecular
236 Graphics System v2.3.4 [42].

237 **RESULTS & DISCUSSION**

238 ***Activity on Chloroform and 1,1,1-Trichloroethane (Methyl Chloroform)***

239 Despite CF and 1,1,1-TCA differing by only one methyl group, RDase activity varies
240 significantly between these compounds. Figure 1 and Table 1 show that TmrA and AcdA have
241 much higher V_{max} and lower K_M values with CF than 1,1,1-TCA. Conversely, CfrA dechlorinates
242 CF and 1,1,1-TCA as substrates at similar rates, but still with a lower K_M for CF. This affinity
243 trend aligns with previously published data despite the greater absolute values (Table 1) [29,43,44].

244 The maximum rates observed for the purified enzymes are 500–100-fold greater than the literature
245 values. Differences in assay setup and the catalyst could cause this. Most of the previous data was
246 performed with cell-free lysates [6,28,29,44], in which the RDase concentration is unknown, causing
247 underestimations of the rate. Additionally, there may be protein-protein interactions in the cell
248 lysate that alter protein-substrate affinity not captured in pure protein. TmrA purified from
249 *Dehalobacter* also had a lower affinity and rate [21]. The reaction time may also cause these
250 discrepancies—previous data was measured from 1-5 h incubations [6,21,28,44]. A long incubation time
251 underestimates the rate because the substrate and electron donor are depleted over time causing
252 the RDase rate to decrease from its initial rate.

253 TmrA and AcdA's higher affinities for CF than 1,1,1-TCA suggest that they have a more
254 compact active site than CfrA, whose difference in K_M is not as drastic. Although, at high
255 concentrations of CF, TmrA and AcdA experience substrate inhibition. Substrate inhibition occurs
256 when the substrate binds unproductively and prevents catalysis, thereby reducing enzyme activity
257 as substrate concentration increases. A low $K_{I,sub}$ corresponds to stronger inhibition because the
258 value represents the concentration needed to reduce the enzyme to half of its maximum rate. This
259 principle is the same for external inhibitors. With a lower $K_{I,CF}$, AcdA experiences stronger
260 substrate inhibition, but at concentrations of CF sub 100 μM the rate is comparable to TmrA
261 (Figure 1A).

262 In published data, cell-free extracts containing CfrA were observed to have inhibition by
263 1,1,1-TCA with a $K_{I,sub}$ range of 300–1000 μM [28,44]. In this work, efforts to fit the 1,1,1-TCA
264 kinetic data with a substrate-inhibition model were unsuccessful, likely due to variance in reaction
265 rate. This variance could be caused by electron donor consumption by 1,1,1-TCA abiotic
266 degradation products, or by the low solubility of 1,1,1-TCA [35,36]. 1,1,1-TCA has a low solubility

(~9 mM) in water [45], and though the tested concentrations are within this threshold, the buffer could interfere with the solubility reducing the concentration available for reaction. The cell-free extract experiments could have suffered from the same confounding variables.

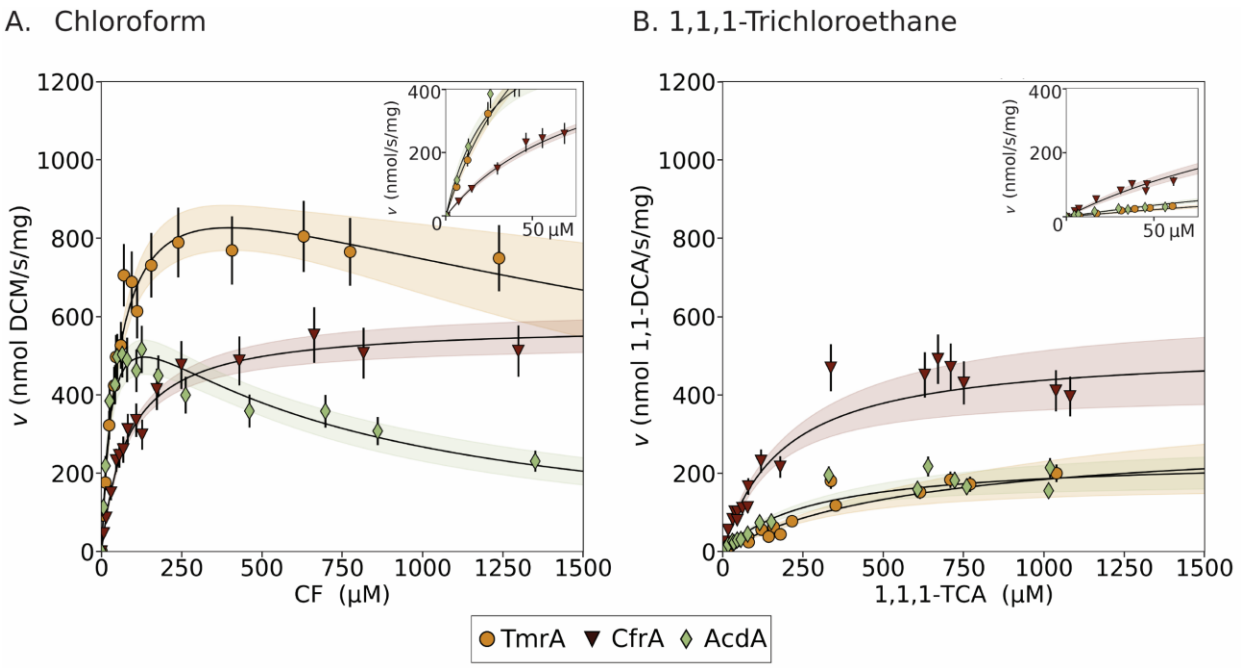

Figure 1. Kinetic curves for TmrA (yellow circles), CfrA (red triangles), and AcdA (green diamonds) using (A) chloroform (CF) and (B) 1,1,1-trichloroethane (1,1,1-TCA) as substrates. Inset plots show the rate of reaction for substrate concentrations lower than 70 μM. Error bars represent the uncertainty in the calculated rate. The black lines are the optimized kinetic models, shaded area represents the 95% confidence interval. All reactions were 2 min at 24°C.

281 **Table 1.** Kinetic parameters with chloroform and 1,1,1-trichloroethane, error is the 95%
282 confidence interval.

RDase	Chloroform				1,1,1-Trichloroethane			Reference
	K_M (μM)	V_{max} (nmol/s/mg)	k_{cat} (s^{-1})	$K_{I,CF}$ (μM)	K_M (μM)	V_{max} (nmol/s/mg)	k_{cat} (s^{-1})	
CfrA	82 ± 12	580 ± 40	28 ± 2	n.o.	180 ± 60	520 ± 100	25 ± 5	This study, refer to Figure 1
	n.t.	n.t.			45 ± 18 *	1.78 ± 0.65 *		Grostern, 2009 [28]
	22 ± 2.4 *	0.32 ± 0.01 *		n.o.	42 ± 6 *	1.7 ± 0.1 *		Wei, 2016 [29]
	28 ± 4 *	1.3 ± 0.1 *		n.o.	34 ± 27 *	1.8 ± 0.9 *		Grostern, 2010 [44]
TmrA	61 ± 14	1100 ± 160	53 ± 8	2600 ± 1900	630 ± 340	300 ± 130	14 ± 6	This study, refer to Figure 1
	154 ± 41	21 ± 2	1.0 ± 0.1	354	n.t.	n.t.		Jugder, 2017 [21]
	30 ± 12 *	2.7 ± 0.2 *		n.o.	237 ± 53 *	0.55 ± 0.05 *		Wong, 2016 [6]
AcdA	29 ± 8	710 ± 120	34 ± 6	610 ± 240	280 ± 100	240 ± 50	12 ± 2	This study, refer to Figure 1

283 * measured from cell-free extracts, n.o. = not observed, n.t. = not tested

284

285 ***Trends of Activity on Native Substrates and Correlation with Kinetic Isotope Effects***

286 The kinetic trends observed for each RDase correlate to the substrate structural differences
287 and the enrichments from which the RDase was identified. The RDases generally exhibit higher
288 V_{max} and lower K_M values with CF, likely due to CF's smaller size facilitating better fit into the
289 active site and faster reaction rates. Both TmrA and AcdA were identified from *Dehalobacter*
290 originating from CF-contaminated sites [12–14,22], while CfrA comes from a *Dehalobacter* enriched

291 from a 1,1,1-TCA and TCE-contaminated site [11]. CfrA, having been the only of these exposed to
292 1,1,1-TCA, may have evolved a specialization resulting in a higher rate than the other two.

293 We can compare these kinetic trends with isotope effects, represented by the enrichment
294 factor (ε). ε reflects how substrates with light isotopes (C^{12}/Cl^{35}) in reactive bonds (those forming
295 or breaking) react faster, enriching the substrate pool with heavier isotopes (C^{13}/Cl^{37}) [46]. These
296 three enzymes are known to produce distinct isotope fractionation patterns when tested *in vivo*
297 [23,24]. Table 2 shows published values of ε for each enzyme—negative values indicate the
298 enrichment of the heavy isotope; a positive value is an inverse isotope effect when the light isotope
299 is enriched [23]. Differences in isotope fractionation can occur due to mechanistic differences in the
300 catalytic slow-step or from "masking effects", which are slow pre-transformation steps that cause
301 suppression of the isotope fractionation. Commitment to catalysis—where substrate binding and
302 catalysis are much faster than substrate dissociation, reducing isotope discrimination—is one such
303 effect (explained further here [23,46,47]).

304 The variance in ε values observed for CfrA, TmrA, and AcdA may result from different
305 transformation mechanisms or structural changes causing masking [24]. Although we cannot
306 determine mechanisms from this kinetic analysis, we can compare catalytic efficiency (k_{cat}/K_M).
307 The k_{cat}/K_M reflects the enzyme's maximum rate and binding affinity. Generally, the k_{cat}/K_M
308 increases in the same order that the $\varepsilon^{13}C$ decreases (Table 2). CfrA has similar fractionation values
309 to the abiotic reaction catalyzed by reduced cobalamin, but TmrA and AcdA have high suppression
310 [23,24]. This suppression may result from higher commitments to catalysis, given that they have
311 higher k_{cat}/K_M values than CfrA. This trend is less clear in the $\varepsilon^{37}Cl$ values due to TmrA's inverse
312 fractionation. Structural diversity between the RDases has been thought to cause these
313 fractionation differences and would also impact their catalytic efficiency [24].

314 **Table 2.** The most recently published carbon and chlorine fractionation values for chloroform and

315 the catalytic efficiency measured in this study; error is the 95% confidence interval.

Catalyst (culture)	$\varepsilon^{13}C$	$\varepsilon^{37}Cl$	k_{cat}/K_M (s^{-1} μM^{-1})	Reference for epsilons
Abiotic				
CNCbl	-26.04 ± 0.91‰	-4.00 ± 0.2‰		Heckel, 2019[23]
CfrA				
(ACT-3)	-26.8 ± 3.2‰	-6.86 ± 0.35‰	0.34 ± 0.06	Phillips, 2022[24]
TmrA				
(CFH2)	-3.1 ± 0.5‰	2.5 ± 0.3‰	0.87 ± 0.24	Heckel, 2019[23]
AcdA				
(SC05)	-1.52 ± 0.34‰	-1.84 ± 0.19v	1.2 ± 0.4	Phillips, 2022[24]

316 CNCbl = cyanocobalamin

317 ***Trichloroethene Inhibition***

318 The inhibition of chloroethenes on chloroalkane reductive dechlorination and vice versa is

319 well established at both the organism and enzyme level [11,28,48–50]. For example, CF will potently

320 inhibit each dechlorination step of TCE by *Dehalococcoides* [29,49,50]; meanwhile, TCE and its

321 dechlorinated products inhibit CfrA activity on CF [28,29]. This reciprocal inhibition may cause a

322 stalemate where no dechlorination occurs. To explore this interaction on other chloroform RDases,

323 we assessed the inhibition of CF-dechlorination in the presence of ~45 μM TCE, simulating

324 conditions where TCE dechlorination is stalled. Although this is not an exhaustive assessment of

325 inhibition, thus the $K_{I,TCE}$ values are less certain, it provides perspective into the differences in

326 sensitivity between the three RDases to external inhibition.

327 All three enzymes showed better model fits with uncompetitive inhibition, as was

328 previously reported for CfrA [29]. AcdA had the most drastic decrease in apparent activity (Figure

329 2); CfrA and TmrA had similar inhibition. CfrA's $K_{I,TCE}$ value was higher but in the same

330 magnitude as that measured in cell-free extracts of $K_{I,TCE}$ of 40 ± 3 μM indicating that this
331 assessment provides a good estimate of inhibition [29]. While TCE inhibition is expected, the
332 inhibition of AcdA at lower TCE concentrations than TmrA and CfrA should be considered when
333 deployed in the field. Additionally, full inhibition studies should be conducted to gain more
334 confidence in the $K_{I,TCE}$ values and assess inhibition by other co-contaminants.
335

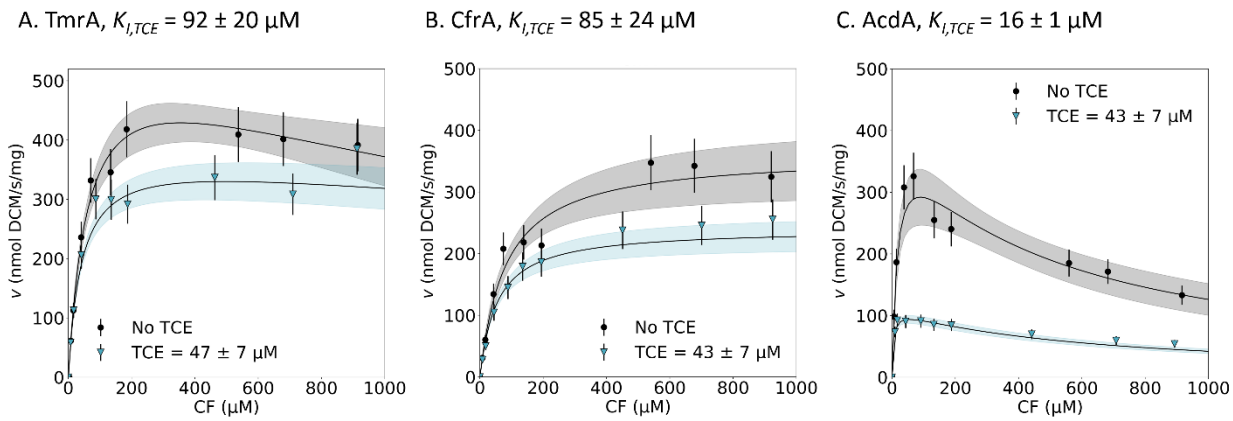

336

337 **Figure 2.** Kinetic curves for TmrA (A), CfrA (B), and AcdA (B) using chloroform (CF) as a
338 substrate with trichloroethane (TCE) inhibition (blue triangle) and without (black circle). The
339 average concentration of TCE between all reactions is presented on each plot, the error represents
340 the standard deviation. Error bars represent the uncertainty in calculated rate. The black lines show
341 the optimized kinetic model**,** shaded area represents the 95% confidence interval. All reactions
342 were 2 min at 20°C.

343 ***Kinetics on 1,1,2-Trichloroethane***

344 1,1,2-TCA is a peculiar substrate because it can undergo both the typical hydrogenolysis
345 to form 1,2-DCA or dihaloelimination to form vinyl chloride (VC). The dihaloelimination of 1,1,2-
346 TCA is strongly favoured as it has a much higher redox potential (E_0' = 1063 mV, H_2 as donor)
347 than the hydrogenolysis reaction (862 mV) [51]. Dihaloelimination can occur abiotically by reduced

348 cobalamin at room temperature and neutral pH [26], it has also been observed by many RDases of
349 varying specificities and likely occurs easily once the substrate enters the active site [19,26]. Enzymes
350 in OG 97 are known to catalyze both reactions, but the product of 1,1,2-TCA dechlorination can
351 be consequential as VC is of higher regulatory concern and inhibits the dechlorination of co-
352 contaminants CF and 1,1,1-TCA [28,29].

353 TmrA has the fastest turnover rate of 1,1,2-TCA, with over double the V_{max} of CfrA and
354 AcdA (Figure 3A, Table 3). AcdA shows the strongest substrate affinity, while CfrA has the largest
355 K_M, nearly ten times higher than AcdA. Regardless of the overall transformation of 1,1,2-TCA, it
356 is important to look at the production rate of the two products, 1,2-DCA and VC, separately. TmrA
357 still achieves the fastest rate of hydrogenolysis to 1,2-DCA (Figure 3B, Table 3). Both TmrA and
358 AcdA perform dihaloelimination to produce VC with similar V_{max} values, but AcdA slightly
359 favours this reaction over hydrogenolysis, resulting in VC as the major product. In contrast, CfrA
360 produces negligible amounts of VC. This homogenous production of 1,2-DCA simplifies
361 subsequent remediation steps and minimizes VC inhibition of other dechlorination processes.
362 Despite its slower rate under field-relevant conditions, CfrA exhibits the most desirable activity
363 against 1,1,2-TCA.

364 Interestingly, the product composition remains consistent for each enzyme across 1,1,2-
365 TCA concentrations and incubation times (Figure S11, Table 3). CfrA produces 98.7 ± 0.6% 1,2-
366 DCA; consistent with 98.8 ± 0.5% previously measured from cell-free extracts [26]. The 1,2-DCA
367 composition produced by TmrA (72 ± 1%) and AcdA (41.2 ± 0.5%) is within 4% of published
368 values performed with longer incubation times [22,26]. This consistency across varying conditions
369 suggests the product distribution is inherent to each OG 97 enzyme and potentially predictable
370 based on structural features controlling it.

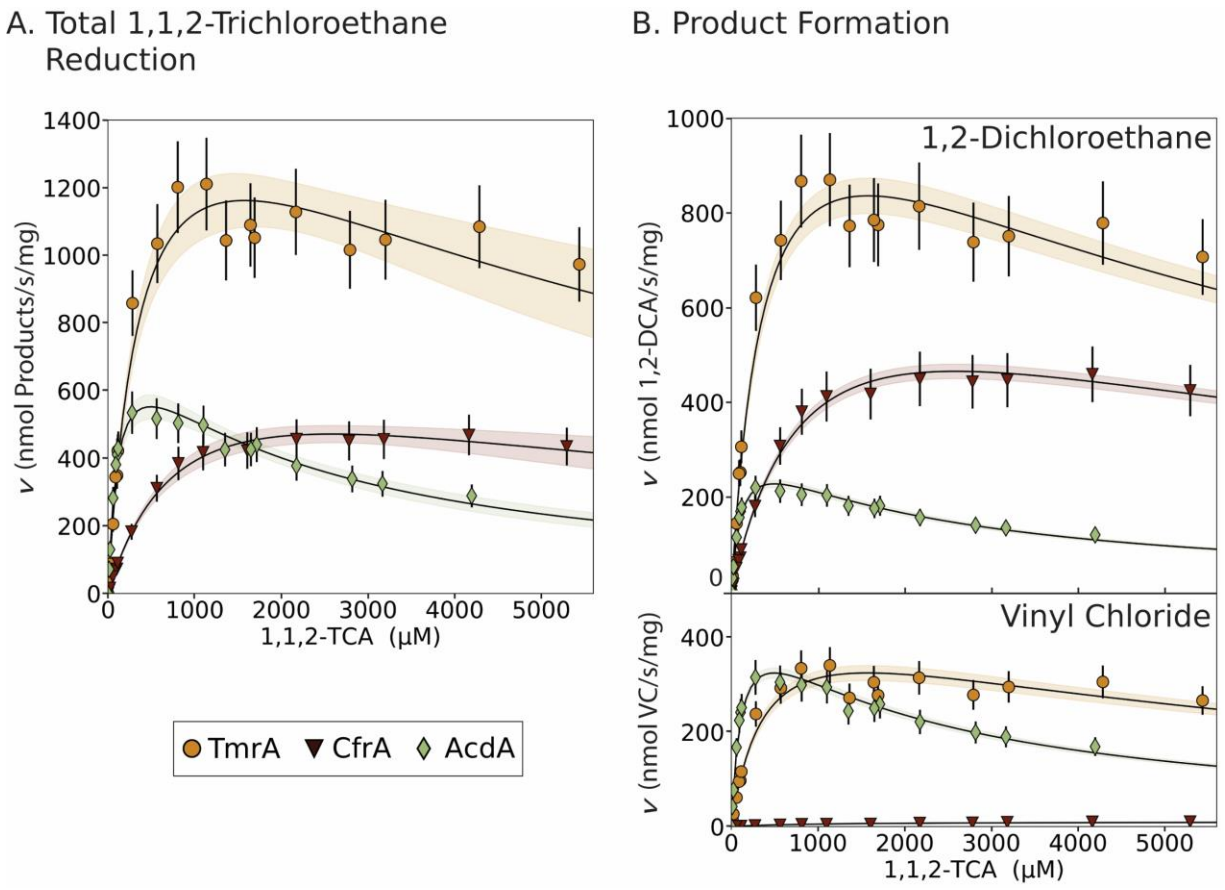

Figure 3. Kinetic curves for TmrA (yellow circles), CfrA (red triangles), and AcdA (green diamonds) using 1,1,2-trichloroethane (1,1,2-TCA) as a substrate. (A) is the total reduction of 1,1,2-trichloroethane and (B) is the production of 1,2-dichloroethane (1,2-DCA; top) and vinyl chloride (VC; bottom). Error bars represent the propagated uncertainty in the reaction rate. The black lines show the optimized kinetic model, shaded area represents the 95% confidence interval. All reactions were 5 min at 24°C.

382 **Table 3.** Kinetic parameters for 1,1,2-trichloroethane as a substrate resulting in either 1,2-
383 dichloroethane or vinyl chloride as products, error is the 95% confidence interval.

RDase	K_M (μM)	$K_{I,TCA}$ (μM)	Total V_{max} (nmol/s/mg)	Total k_{cat} (s^{-1})	1,2-DCA V_{max} (nmol/s/mg)	1,2-DCA k_{cat} (s^{-1})	VC V_{max} (nmol/s/mg)	VC k_{cat} (s^{-1})	Percent of 1,2-DCA in product (%)
CfrA	950 ± 220	7100 ± 4400	820 ± 160	39 ± 4	810 ± 20	38 ± 0.5	10 ± 0.6	0.48 ± 0.01	98.7 ± 0.6
TmrA	400 ± 96	6200 ± 3700	1800 ± 320	86 ± 8	1300 ± 50	62 ± 1	490 ± 20	24 ± 0.5	72.0 ± 1.1
AcdA	120 ± 20	2000 ± 550	820 ± 100	39 ± 2	340 ± 10	16 ± 0.5	480 ± 15	23 ± 0.5	41.2 ± 0.5

384 TCA = trichloroethane, DCA = dichloroethane, VC = vinyl chloride
385

386 ***Variance In Catalytic Residues***

387 Despite over 95% amino acid sequence identity equating only 15–21 amino acid
388 differences (Supplemental Text S7), CfrA, TmrA, and AcdA exhibit distinct kinetic
389 characteristics. Since these enzymes were all expressed heterologously, these differences must be
390 attributed to the peptide sequence rather than variations within the actual organism—such as the
391 type of cobamide used, which can affect the dechlorination activity [52–54]. Although experimentally
392 derived structures of chloroalkane reductases remain elusive, protein modelling offers some
393 insights. The resolution of the PceA (*Sulfurospirillum multivorans*) crystal structure revealed
394 several highly conserved active site residues critical for activity [41,55]. Many differences we observe
395 between the OG 97 RDases overlap or collocate with these important residues. The identity of
396 residues involved in protonation during hydrogenolysis is of particular interest as they directly
397 impact the dehalogenation reaction and, therefore, the rate.

398 PceA features a tyrosine (Tyr246) at the substrate binding site, long thought to be the
399 primary proton donor due to its position and necessity for enzyme activity and conservation in
400 many RDases including those from *Dehalococcoides* and *Dehalobacter* (Supplementary Text S7)
401 [19,41]. Mutagenic studies also implicated a neighbouring asparagine Asn272 and arginine Arg305 in
402 catalysis [19,41,55], believed to stabilize Tyr246 via H-bonding, evident from their proximity in crystal
403 structures (~3 Å; Figure 4A). However, a recent computational study by Zhang *et al.* suggests the
404 more energetically favourable proton donor is Arg305, with Tyr246 and Asn272 positioning
405 Arg305 toward the substrate [56].

406 This hypothesis better explains the activity of CfrA and TmrA, which lack tyrosine at the
407 expected position but have the arginine Arg319 (Figure 4B/C). TmrA instead has a non-H-bonding
408 phenylalanine (Phe260) and CfrA has a cysteine (Cys260), which may have a weaker H-bond due
409 to the distance (3.3 Å in the model) and leaves a larger space in the active site. Both enzymes have
410 serine (Ser286) instead of Asn272, capable of H-bonding. AcdA retains the conserved tyrosine
411 (Tyr260) and arginine (Arg319) but has alanine (Ala286) instead of asparagine (Figure 4D). This
412 asparagine is less conserved in RDases (Supplemental Text S7), so its exact role is unclear, but a
413 network of interactions could potentially affect the catalytic residue positioning relative to
414 substrates.

415 Regardless of their high sequence identity, TmrA, CfrA, and AcdA have drastic differences
416 in these ostensibly highly conserved residues that likely influence their kinetic properties. For
417 instance, an aromatic residue in position 260 may support a tighter interaction with the substrates
418 leading to TmrA and AcdA having lower K_M values for CF and 1,1,2-TCA than CfrA (more detail
419 in Supplemental Text S7). Phillips *et al.* also identified other residues (Tyr80, Leu388, and Met391
420 in CfrA; Phe80, Phe388, and Trp391 in TmrA and AcdA) as possible sources of isotopic

421 fractionation variance [24]. Future mutant studies should explore these catalysis-implicated residues

422 to understand their impact on kinetic characteristics and isotope effects.

423

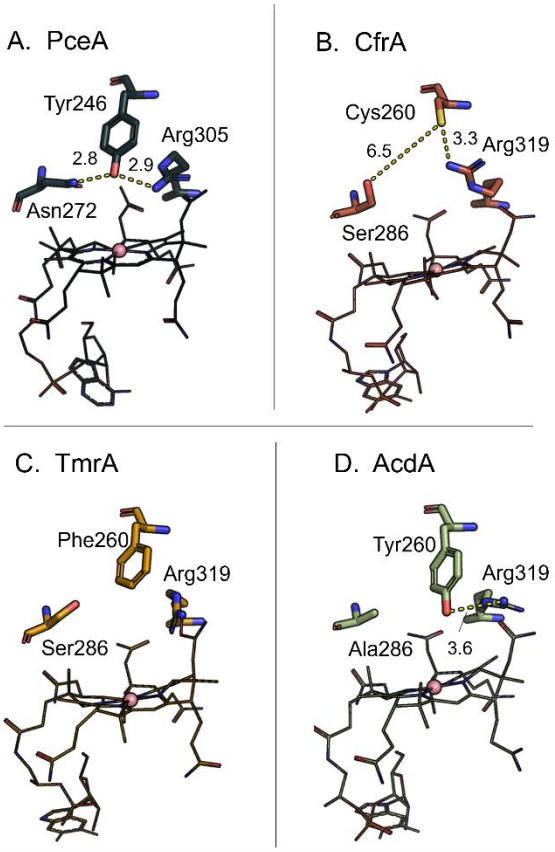

424

425 **Figure 4.** The conserved active site residues in the PceA crystal structure with predicted catalytic

426 activity and the corresponding residues in CfrA, TmrA, and AcdA protein models. Distances

427 between key residues are shown as dashed lines with the distance in angstroms. Wire structure is

428 the cobamide cofactor and the pink sphere is the cobalt. PDB ID: 4ur0 [41].

429 ***Implications For Bioremediation***

430 This is the first true comparative kinetic study of highly similar purified RDases, revealing

431 that even near-identical RDase variants can exhibit distinct behaviours that could influence

432 remediation processes. First, kinetic parameters can be incorporated into groundwater models to

433 help interpret field data and improve predictions of remedial progress. For example, establishing
434 enzymatic rates can be useful for monitoring natural attenuation. Recent studies used quantitative
435 PCR and proteomics to quantify active RDases in aquifers [57,58]. By combining RDase and substrate
436 concentrations with kinetic parameters, degradation rates (yr^{-1}) can be predicted using the
437 Michaelis-Menten model [57,58]. Predicting rates is necessary for decision-making at contaminant
438 sites, and expanding the library of RDase kinetic coefficients will facilitate the implementation of
439 this technique across more compounds.

440 Understanding the link between RDase sequence and associated differences in activity in
441 terms of substrate preferences, products and inhibitors will aid in the interpretation field data at
442 contaminated sites. Sequence variants of closely related RDases are sometimes detected at field
443 sites, but their impact is generally not considered in interpreting results; the published features of
444 the RDase is assumed without consideration to possible differences due to sequence variants.
445 However, as molecular tools become more accessible, sequence variants will be more easily
446 detected. For example, sequence variants within OG 97 were detected at a 1,1,1-TCA-
447 contaminated site and shown to correlate with activity on either 1,1,1-TCA or 1,1-DCA substrates
448 [59]. The different rates and sensitivity to common inhibitors found here likely extend to other OGs,
449 highlighting the need for further comparative studies. Knowledge of RDase variant kinetics and
450 inhibition could explain why natural attenuation sometimes stalls despite the presence of
451 dechlorinators and appropriate RDases. If inhibition is an issue, biostimulation strategies would
452 be ineffective, requiring alternatives for alleviating the inhibition [50].

453 Furthermore, this work outlines an accurate syringe barrel method for directly assay
454 enzyme kinetics, expediting inhibitor screening, and revealing functional differences between
455 RDases and organohalide respirers. Investigating the structural basis for kinetic variation will

456 elucidate significant active site residues and guide future selection or engineering of more efficient
457 RDases.

458 **ACKNOWLEDGEMENTS**

459 This study was supported by the Government of Ontario with an Ontario Graduate
460 Scholarship to K.J.P, by the Natural Science and Engineering Research Council (NSERC) with a
461 Discovery Grant to E.A.E and a Canadian Research Chair to E.A.E. We thank the Booker Lab
462 (Pennsylvania State University), the Antony Lab (St. Louis University School of Medicine), and
463 the Kiley lab (University of Wisconsin-Madison) for gifting materials.

464 **ASSOCIATED CONTENT**

465 **Supporting Information**.

466 Detailed methods for RDase production, additional assay details, and equations and explanations
467 for all kinetic models used, discussion about the temperature dependence observed, graphical
468 representations of the raw data and substrate conversion, and amino acid sequence alignments
469 of RDases to complement structural comparison. (PDF)

470 All raw data for the assays run, including the negative controls, and all of the parameters and
471 statistical values for each model fitting. (XLSX)

472 **AUTHOR INFORMATION**

473 **Corresponding Author**

474 Elizabeth A. Edwards - *Department of Chemical Engineering and Applied Chemistry, University*
475 *of Toronto, Toronto, Ontario, Canada M5S 3E5*; orcid.org/0000-0002-8071-338X; Email:
476 elizabeth.edwards@utoronto.ca.

Authors

Katherine J. Picott – *Department of Chemical Engineering and Applied Chemistry, University of Toronto, Toronto, Ontario, Canada M5S 3E5;* orcid.org/0000-0003-3525-2366

Author Contributions

E.A.E. and K.J.P. conceived of the project. All experiments and data analysis were carried out by K.J.P. The manuscript was written through contributions of all authors. All authors have given approval to the final version of the manuscript.

Notes

The authors declare no competing financial interest.

REFERENCES

(1) Agency for Toxic Substances and Disease Registry (ATSDR). ATSDR's Substance Priority List. https://www.atsdr.cdc.gov/spl/index.html.

(2) Koenig, J.; Lee, M.; Manefield, M. Aliphatic Organochlorine Degradation in Subsurface Environments. *Rev. Environ. Sci. Biotechnol.* **2015**, *14* (1), 49–71. https://doi.org/10.1007/s11157-014-9345-3.

(3) Amber, W. R.; Aziz, C. E.; Bruce, C. L.; Cox, E.; Criddle, C. S.; Dybas, M. J.; Edwards, E. A.; Giddings, C. G. S.; Gossett, J. M.; Harkness, M.; et al. *Bioaugmentation for Groundwater Remediation*; Stroo, H. F., Leeson, A., Ward, C. H., Eds.; Springer, 2013.

(4) Edwards, E. A.; Löffler, F. E. Harnessing Microbial Activities for Environmental Cleanup. *Curr. Opin. Biotechnol.* **2006**, *17*, 274–284. https://doi.org/10.1016/j.copbio.2006.05.001.

498 (5) Xiao, Z.; Jiang, W.; Chen, D.; Xu, Y. Bioremediation of Typical Chlorinated Hydrocarbons
499 by Microbial Reductive Dechlorination and Its Key Players: A Review. *Ecotoxicol.*
500 *Environ. Saf.* **2020**, *202*, 110925. https://doi.org/10.1016/j.ecoenv.2020.110925.

501 (6) Wong, Y. K.; Holland, S. I.; Ertan, H.; Manefield, M.; Lee, M. Isolation and
502 Characterization of *Dehalobacter* sp. Strain UNSWDHB Capable of Chloroform and
503 Chlorinated Ethane Respiration. *Environ. Microbiol.* **2016**, *18*, 3092–3105.
504 https://doi.org/10.1111/1462-2920.13287.

505 (7) Ding, C.; Zhao, S.; He, J. A *Desulfitobacterium* sp. Strain PR Reductively Dechlorinates
506 Both 1,1,1-Trichloroethane and Chloroform. *Environ. Microbiol.* **2014**, *16* (11), 3387–
507 3397. https://doi.org/10.1111/1462-2920.12387.

508 (8) Zhao, S.; Ding, C.; He, J. Detoxification of 1,1,2-Trichloroethane to Ethene by
509 *Desulfitobacterium* and Identification of Its Functional Reductase Gene. *PLoS One* **2015**,
510 *10* (4), e0119507. https://doi.org/10.1371/journal.pone.0119507.

511 (9) Zhao, S.; Rogers, M. J.; He, J. Microbial Reductive Dehalogenation of Trihalomethanes by
512 a *Dehalobacter*-Containing Co-Culture. *Appl. Microbiol. Biotechnol.* **2017**, *101* (13), 5481–
513 5492. https://doi.org/10.1007/s00253-017-8236-2.

514 (10) Soder-Walz, J. M.; Torrentó, C.; Algora, C.; Wasmund, K.; Cortés, P.; Soler, A.; Vicent,
515 T.; Rosell, M.; Marco-Urrea, E. Trichloromethane Dechlorination by a Novel *Dehalobacter*
516 sp. Strain 8M Reveals a Third Contrasting C and Cl Isotope Fractionation Pattern within
517 This Genus. *Sci. Total Environ.* **2022**, *813*, 152659.
518 https://doi.org/10.1016/j.scitotenv.2021.152659.

519 (11) Grostern, A.; Edwards, E. A. A 1,1,1-Trichloroethane-Degrading Anaerobic Mixed
520 Microbial Culture Enhances Biotransformation of Mixtures of Chlorinated Ethenes and
521 Ethanes. *Appl. Environ. Microbiol.* **2006**, *72* (12), 7849–7856.
522 https://doi.org/10.1128/AEM.01269-06.

523 (12) Lee, M.; Low, A.; Zemb, O.; Koenig, J.; Michaelsen, A.; Manefield, M. Complete
524 Chloroform Dechlorination by Organochlorine Respiration and Fermentation. *Environ.*
525 *Microbiol.* **2012**, *14*, 883–894. https://doi.org/10.1111/j.1462-2920.2011.02656.x.

526 (13) Wang, H.; Yu, R.; Webb, J.; Dollar, P.; Freedman, D. L. Anaerobic Biodegradation of
527 Chloroform and Dichloromethane with a *Dehalobacter* Enrichment Culture. *Appl. Environ.*
528 *Microbiol.* **2022**, *88* (4), e01970-21. https://doi.org/10.1128/aem.01970-21.

529 (14) Bulka, O.; Webb, J.; Dworatzek, S.; Mahadevan, R.; Edwards, E. A. A Multifunctional
530 *Dehalobacter*? Tandem Chloroform and Dichloromethane Degradation in a Mixed
531 Microbial Culture. *Environ. Sci. Technol.* **2023**, *57* (48), 19912–19920.
532 https://doi.org/10.1021/acs.est.3c06686.

533 (15) Fincker, M.; Spormann, A. M. Biochemistry of Catabolic Reductive Dehalogenation. *Annu.*
534 *Rev. Biochem.* **2017**, *86* (1), 357–386. https://doi.org/10.1146/annurev-biochem-061516-
535 044829.

536 (16) Hug, L. A.; Maphosa, F.; Leys, D.; Löffler, F. E.; Smidt, H.; Edwards, E. A.; Adrian, L.
537 Overview of Organohalide-Respiring Bacteria and a Proposal for a Classification System
538 for Reductive Dehalogenases. *Philos. Trans. R. Soc. B* **2013**, *368*, 20120322.

539 (17) Molenda, O.; Puentes Jácome, L. A.; Cao, X.; Nesbø, C. L.; Tang, S.; Morson, N.; Patron,

540 J.; Lomheim, L.; Wishart, D. S.; Edwards, E. A. Insights into Origins and Function of the
541 Unexplored Majority of the Reductive Dehalogenase Gene Family as a Result of Genome
542 Assembly and Ortholog Group Classification. *Environ. Sci. Process. Impacts* **2020**, *22* (3),
543 663–678. https://doi.org/10.1039/c9em00605b.

544 (18) Alfán-Guzmán, R.; Ertan, H.; Manefield, M.; Lee, M. Isolation and Characterization of
545 *Dehalobacter* sp. Strain TeCB1 Including Identification of TcbA: A Novel Tetra- and
546 Trichlorobenzene Reductive Dehalogenase. *Front. Microbiol.* **2017**, *8* (April), 558.
547 https://doi.org/10.3389/fmicb.2017.00558.

548 (19) Kunze, C.; Diekert, G.; Schubert, T. Subtle Changes in the Active Site Architecture
549 Untangled Overlapping Substrate Ranges and Mechanistic Differences of Two Reductive
550 Dehalogenases. *FEBS J.* **2017**, *284* (20), 3520–3535. https://doi.org/10.1111/febs.14258.

551 (20) Tang, S.; Edwards, E. A. Identification of *Dehalobacter* Reductive Dehalogenases That
552 Catalyse Dechlorination of Chloroform, 1,1,1- Trichloroethane and 1,1-Dichloroethane.
553 *Philos. Trans. R. Soc. B* **2013**, *368* (1616), 20120318.
554 https://doi.org/10.1098/rstb.2012.0318.

555 (21) Jugder, B. E.; Bohl, S.; Lebhar, H.; Healey, R. D.; Manefield, M.; Marquis, C. P.; Lee, M.
556 A Bacterial Chloroform Reductive Dehalogenase: Purification and Biochemical
557 Characterization. *Microb. Biotechnol.* **2017**, *10* (6), 1640–1648.
558 https://doi.org/10.1111/1751-7915.12745.

559 (22) Bulka, O.; Picott, K.; Mahadevan, R.; Edwards, E. A. From *mec* Cassette to *rdhA*: A Key
560 *Dehalobacter* Genomic Neighborhood in a Chloroform and Dichloromethane–
561 Transforming Microbial Consortium. *Appl. Environ. Microbiol.* **2024**, *90* (6), e00732-24.

562 https://doi.org/https://doi.org/10.1128/aem.00732-24.

563 (23) Heckel, B.; Phillips, E.; Edwards, E.; Sherwood Lollar, B.; Elsner, M.; Manefield, M. J.;
564 Lee, M. Reductive Dehalogenation of Trichloromethane by Two Different *Dehalobacter*
565 *restrictus* Strains Reveal Opposing Dual Element Isotope Effects. *Environ. Sci. Technol.*
566 **2019**, *53* (5), 2332–2343. https://doi.org/10.1021/acs.est.8b03717.

567 (24) Phillips, E.; Bulka, O.; Picott, K.; Kümmel, S.; Edwards, E. A.; Nijenhuis, I.; Gehre, M.;
568 Dworatzek, S.; Webb, J.; Sherwood Lollar, B. Investigation of Active Site Amino Acid
569 Influence on Carbon and Chlorine Isotope Fractionation during Reductive Dechlorination.
570 *FEMS Microbiol. Ecol.* **2022**, *98* (8), fiac072. https://doi.org/10.1093/femsec/fiac072.

571 (25) Jugder, B.; Ertan, H.; Bohl, S.; Lee, M.; Marquis, C. P.; Manefield, M. Organohalide
572 Respiring Bacteria and Reductive Dehalogenases: Key Tools in Organohalide
573 Bioremediation. *Front. Microbiol.* **2016**, *7* (March), 249.
574 https://doi.org/10.3389/fmicb.2016.00249.

575 (26) Picott, K. J.; Flick, R.; Edwards, E. A. Heterologous Expression of Active *Dehalobacter*
576 Respiratory Reductive Dehalogenases in *Escherichia coli*. *Appl. Environ. Microbiol.* **2022**,
577 *88* (3), e01993-21. https://doi.org/10.1128/AEM.01993-21.

578 (27) Jugder, B.-E.; Payne, K. A. P.; Fisher, K.; Bohl, S.; Lebhar, H.; Manefield, M.; Lee, M.;
579 Leys, D.; Marquis, C. P. Heterologous Production and Purification of a Functional
580 Chloroform Reductive Dehalogenase. *ACS Chem. Biol.* **2018**, *13*, 548–552.
581 https://doi.org/10.1021/acschembio.7b00846.

582 (28) Grostern, A.; Chan, W. W. M.; Edwards, E. A. 1,1,1-Trichloroethane and 1,1-

583 Dichloroethane Reductive Dechlorination Kinetics and Co-Contaminant Effects in a
584 *Dehalobacter*-Containing Mixed Culture. *Environ. Sci. Technol.* **2009**, *43* (17), 6799–6807.

585 (29) Wei, K.; Grostern, A.; Chan, W. W. M.; Richardson, R. E.; Edwards, E. A. Electron
586 Acceptor Interactions Between Organohalide-Respiring Bacteria: Cross-Feeding,
587 Competition, and Inhibition. In *Organohalide-Respiring Bacteria*; Springer-Verlag Berlin
588 Heidelberg, 2016; pp 283–308.

589 (30) Corless, E. I.; Mettert, E. L.; Kiley, P. J.; Antony, E. Elevated Expression of a Functional
590 Suf Pathway in *Escherichia coli* BL21(DE3) Enhances Recombinant Production of an Iron-
591 Sulfur Cluster-Containing Protein. *J. Bacteriol.* **2020**, *202* (3), e00496-19.

592 (31) Lanz, N. D.; Blaszczyk, A. J.; McCarthy, E. L.; Wang, B.; Wang, R. X.; Jones, B. S.;
593 Booker, S. J. Enhanced Solubilization of Class B Radical S-Adenosylmethionine
594 Methylases by Improved Cobalamin Uptake in *Escherichia coli*. *Biochemistry* **2018**, *57* (9),
595 1475–1490. https://doi.org/10.1021/acs.biochem.7b01205.

596 (32) Bradford, M. M. A Rapid and Sensitive Method for the Quantitation of Microgram
597 Quantities of Protein Utilizing the Principle of Protein-Dye Binding. *Anal. Biochem.* **1976**,
598 *72*, 248–254. https://doi.org/10.1016/j.cj.2017.04.003.

599 (33) Criddle, C. S. Reductive Dehalogenation in Microbial and Electrolytic Model Systems,
600 Stanford University, 1989.

601 (34) Nijenhuis, I.; Zinder, S. H. Characterization of Hydrogenase and Reductive Dehalogenase
602 Activities of *Dehalococcoides ethenogenes* Strain 195. *Appl. Environ. Microbiol.* **2005**, *71*
603 (3), 1664–1667. https://doi.org/10.1128/AEM.71.3.1664-1667.2005.

604 (35) Gerkens, R. R.; Franklin, J. A. The Rate of Degradation of 1,1,1-Trichloroethane in Water
605 by Hydrolysis and Dehydrochlorination. *Chemosphere* **1989**, *19* (12), 1929–1937.

606 (36) Vogel, T. M.; McCarty, P. L. Abiotic and Biotic Transformations of 1,1,1-Trichloroethane
607 under Methanogenic Conditions. *Environ. Sci. Technol.* **1987**, *21* (12), 1208–1213.
608 https://doi.org/10.1021/es00165a008.

609 (37) Newville, M.; Stensitzki, T.; Allen, D. B.; Ingargiola, A. LMFIT: Non-Linear Least-Square
610 Minimization and Curve-Fitting for Python. 2014.

611 (38) Hekkelman, M. L.; de Vries, I.; Joosten, R. P.; Perrakis, A. AlphaFill: Enriching AlphaFold
612 Models with Ligands and Cofactors. *Nat. Methods* **2023**, *20* (2), 205–213.
613 https://doi.org/10.1038/s41592-022-01685-y.

614 (39) Jumper, J.; Evans, R.; Pritzel, A.; Green, T.; Figurnov, M.; Ronneberger, O.;
615 Tunyasuvunakool, K.; Bates, R.; Žídek, A.; Potapenko, A.; et al. Highly Accurate Protein
616 Structure Prediction with AlphaFold. *Nature* **2021**, *596*, 583–589.
617 https://doi.org/10.1038/s41586-021-03819-2.

618 (40) Krieger, E.; Joo, K.; Lee, J.; Lee, J.; Raman, S.; Thompson, J.; Tyka, M.; Baker, D.; Karplus,
619 K. Improving Physical Realism, Stereochemistry, and Side-Chain Accuracy in Homology
620 Modeling: Four Approaches That Performed Well in CASP8. *Proteins Struct. Funct.*
621 *Bioinforma.* **2009**, *77* (SUPPL. 9), 114–122. https://doi.org/10.1002/prot.22570.

622 (41) Bommer, M.; Kunze, C.; Fesseler, J.; Schubert, T.; Diekert, G.; Dobbek, H. Structural Basis
623 for Organohalide Respiration. *Science* **2014**, *346* (6208), 455–458.

624 (42) Schrödinger LLC. The PyMOL Molecular Graphics System, Version 2.0.

625 (43) Grostern, A.; Edwards, E. A. Characterization of a Dehalobacter Coculture That
626 Dechlorinates 1,2-Dichloroethane to Ethene and Identification of the Putative Reductive
627 Dehalogenase Gene. *Appl. Environ. Microbiol.* **2009**, *75* (9), 2684–2693.
628 https://doi.org/10.1128/AEM.02037-08.

629 (44) Grostern, A.; Duhamel, M.; Dworatzek, S.; Edwards, E. A. Chloroform Respiration to
630 Dichloromethane by a *Dehalobacter* Population. *Environ. Microbiol.* **2010**, *12* (4), 1053–
631 1060. https://doi.org/10.1111/j.1462-2920.2009.02150.x.

632 (45) Mackay, D.; Shiu, W.-Y.; Ma, K.-C.; Lee, S. C. *Handbook of Physical-Chemical Properties*
633 *and Environmental Fate for Organic Chemicals*, 2nd ed.; CRC Press, 2006.

634 (46) Elsner, M.; Zwank, L.; Hunkeler, D.; Schwarzenbach, R. P. A New Concept Linking
635 Observable Stable Isotope Fractionation to Transformation Pathways of Organic Pollutants.
636 *Environ. Sci. Technol.* **2005**, *39*, 6896–6916.

637 (47) Northrop, D. B. The Expression of Isotope Effects on Enzyme-Catalyzed Reactions. *Annu.*
638 *Rev. Biochem.* **1981**, *50*, 103–131. https://doi.org/10.1146/annurev.bi.50.070181.000535.

639 (48) Li, H.; He, J.; Jia, W. The Influence of Gut Microbiota on Drug Metabolism and Toxicity.
640 *Expert Opin. Drug Metab. Toxicol.* **2016**, *12*, 31–40.
641 https://doi.org/10.1517/17425255.2016.1121234.The.

642 (49) Duhamel, M.; Wehr, S. D.; Yu, L.; Rizvi, H.; Seepersad, D.; Dworatzek, S.; Cox, E. E.;
643 Edwards, E. A. Comparison of Anaerobic Dechlorinating Enrichment Cultures Maintained
644 on Tetrachloroethene, Trichloroethene, *cis*-Dichloroethene and Vinyl Chloride. *Water Res.*
645 **2002**, *36*, 4193–4202.

646 (50) Xu, G.; Zhao, S.; Chen, C.; Zhang, N.; He, J. Alleviating Chlorinated Alkane Inhibition on
647 *Dehalococcoides* to Achieve Detoxification of Chlorinated Aliphatic Cocontaminants.
648 *Environ. Sci. Technol.* **2023**, *57* (40), 15112–15122.
649 https://doi.org/10.1021/acs.est.3c04535.

650 (51) Dolfing, J. Energetic Considerations in Organohalide Respiration. In *Organohalide-*
651 *Respiring Bacteria*; Springer, 2016; pp 31–48.

652 (52) Wang, P.-H.; Tang, S.; Nemr, K.; Flick, R.; Yan, J.; Mahadevan, R.; Yakunin, A. F.; Löffler,
653 F. E.; Edwards, E. A. Refined Experimental Annotation Reveals Conserved Corrinoid
654 Autotrophy in Chloroform-Respiring *Dehalobacter* Isolates. *ISME J.* **2017**, *11*, 626–640.
655 https://doi.org/10.1038/ismej.2016.158.

656 (53) Yan, J.; Şimşir, B.; Farmer, A. T.; Bi, M.; Yang, Y.; Campagna, S. R.; Löffler, F. E. The
657 Corrinoid Cofactor of Reductive Dehalogenases Affects Dechlorination Rates and Extents
658 in Organohalide-Respiring *Dehalococcoides mccartyi*. *ISME J.* **2016**, *10* (5), 1092–1101.
659 https://doi.org/10.1038/ismej.2015.197.

660 (54) Yan, J.; Bi, M.; Bourdon, A. K.; Farmer, A. T.; Wang, P.-H.; Molenda, O.; Quaile, A. T.;
661 Jiang, N.; Yang, Y.; Yin, Y.; et al. Purinyl-Cobamide Is a Native Prosthetic Group of
662 Reductive Dehalogenases. *Nat. Chem. Biol.* **2018**, *14*, 8–14.
663 https://doi.org/10.1038/nchembio.2512.

664 (55) Payne, K. A. P.; Quezada, C. P.; Fisher, K.; Dunstan, M. S.; Collins, F. A.; Sjuts, H.; Levy,
665 C.; Hay, S.; Rigby, S. E. J.; Leys, D. Reductive Dehalogenase Structure Suggests a
666 Mechanism for B_{12}-Dependent Dehalogenation. *Nature* **2015**, *517*, 513–516.
667 https://doi.org/10.1038/nature13901.

668 (56) Zhang, X.; Wang, Z.; Li, Z.; Shaik, S.; Wang, B. [4Fe-4S]-Mediated Proton-Coupled
669 Electron Transfer Enables the Efficient Degradation of Chloroalkenes by Reductive
670 Dehalogenases. *ACS Catal.* **2023**, *13*, 1173–1185.
671 https://doi.org/10.1021/acscatal.2c06306.

672 (57) Kucharzyk, K. H.; Murdoch, F. K.; Wilson, J.; Michalsen, M.; Frank, E. L.; Murdoch, R.
673 W.; Istok, J. D.; Hatzinger, P. B.; Mullins, L.; Hill, A. Integrated Advanced Molecular Tools
674 Predict In Situ cVOC Degradation Rates: Field Demonstration. *Environ. Sci. Technol.* **2023**,
675 *58*, 557–569. https://doi.org/10.1021/acs.est.3c06231.

676 (58) Michalsen, M. M.; Kara Murdoch, F.; Löffler, F. E.; Wilson, J.; Hatzinger, P. B.; Istok, J.
677 D.; Mullins, L.; Hill, A.; Murdoch, R. W.; Condee, C.; et al. Quantitative Proteomics and
678 Quantitative PCR as Predictors of *cis*-1,2-Dichlorethene and Vinyl Chloride Reductive
679 Dechlorination Rates in Bioaugmented Aquifer Microcosms. *ACS ES&T Eng.* **2022**, *2*, 43–
680 53. https://doi.org/10.1021/acsestengg.1c00207.

681 (59) Yang, M. I.; Previdsa, M.; Edwards, E. A.; Sleep, B. E. Two Distinct *Dehalobacter* Strains
682 Sequentially Dechlorinate 1,1,1-Trichloroethane and 1,1-Dichloroethane at a Field Site
683 Treated with Granular Zero Valent Iron and Guar Gum. *Water Res.* **2020**, *186*, 116310.
684 https://doi.org/10.1016/j.watres.2020.116310.

685

686

687

688

689

690 **TOC FIGURE**
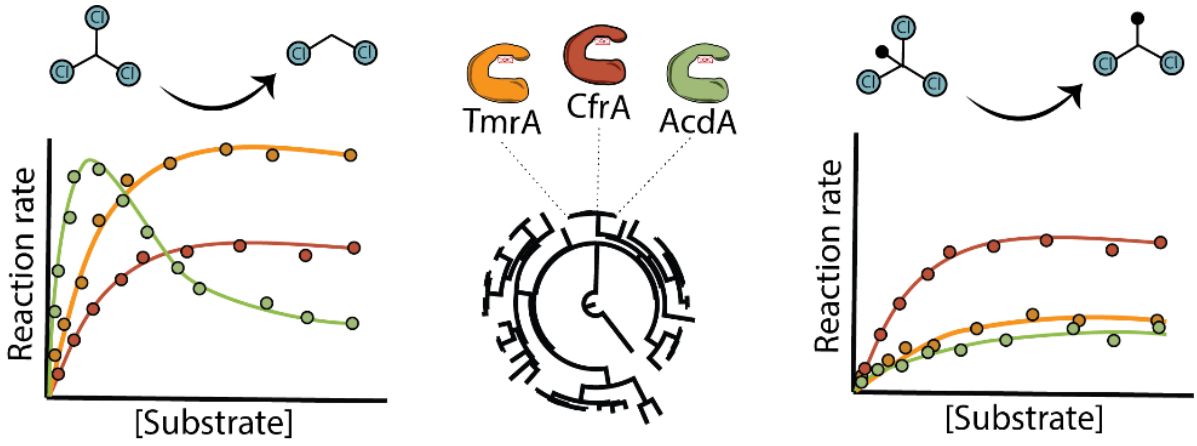
691